Microstructures and electrical properties of Ru-C nano-composite films by PECVD

Materials Transactions, Vol. 48, No. 1 (2007) pp. 58 to 63

Microstructures and Electrical Properties of Ru-C Nano-Composite Films by PECVD

Masato Sakata*, Teiichi Kimura and Takashi Goto

Institute for Materials Research, Tohoku University, 980-8577, Japan

Ruthenium-Carbon (Ru-C) nano-composite films were prepared by plasma-enhanced chemical vapor deposition (PECVD) and the effects of deposition conditions on the microstructure and electrical properies were investigated. The films consisted of agglomerated grains of 10 to 20 nm in diameter, in which Ru particles of 2.5 to 3.5 nm in diameter were dispersed in a C matrix. The C content of the films was about 90 vol%. The electrical properties of Ru-C nano-composite films as a catalytic electrode for an yttria-stabilized zirconia (YSZ) solid electrolyte were evaluated by AC impedance spectroscopy. The interfacial electrical conductivity at the Ru-C/YSZ interface was 0.2×10^{-3} Sm^{-1} at 500 K and increased with increasing temperature. The activation energy of the interfacial electrical conductivity was about 70 kJ/mol, implying an oxygen diffusion limited process at the interface. [doi:10.2320/matertrans.48.58]

(Received July 28, 2006; Accepted November 15, 2006; Published December 25, 2006)

Keywords: *ruthenium-carbon nano-composite, plasma-enhanced chemical vapor deposition, oxygen sensor, impedance spectroscopy, interfacial conductivity*

1. Introduction

A solid-electrolyte-type oxygen sensor basically consists of an electrode and a solid electrolyte, platinum (Pt) and yttria-stabilized zirconia (YSZ) respectively, being commonly employed. The YSZ oxygen sensor is widely used for automobiles because of its superior thermal and chemical stability and can be operated at high temperatures over 1000 K to ensure the catalytic activity of Pt and high mobility of ionic charges in the YSZ solid electrolyte. However, to elongate the lifetime and to reduce the energy consumption of the YSZ sensor, the development of a highly catalytic electrode is required to operate the YSZ sensor at low temperatures.

Pt group metals can be widely employed for the electrode material because of their high electrical conductivity, thermal stability and superior catalytic activity for the dissociation of oxygen molecules.[1] Ruthenium (Ru) may be the most promising electrode material among the Pt group metals for the oxygen sensor due to its low adsorption heat of oxygen molecules.[2,3] Since the electro-motive-force (EMF) of the oxygen sensor is generated by a charge transfer at the electrode/electrolyte/gas triple phase boundary, nano-sized Ru particles are expected to be an excellent electrode material.

Ru thin film has attracted much attention as an electrode material for dynamic random access memories (DRAM) and very large-scale integration (VLSI) circuits due to its high electrical conductivity and thermal stability.[4–7] Highly catalytic activity of Ru thin films prepared by MOCVD have also been reported in a Fischer-Tropsch reaction,[8] ammonia synthesis[9] and oxidation reaction of CO.[10] Recently, a Pt-Ru nano-composite film has been studied as a new electrode material for fuel cells, and its high catalytic activity with excellent chemical stability of Ru particles of several nm in diameter has been reported.[11–14]

Many metallic films have been prepared by metalorganic chemical vapor deposition (MOCVD), in which impurity C has been often contained, mainly due to insufficient oxidant supply during the deposition process. Therefore, the elimination of impurity C has been a significant issue because this impurity C is degrades the electrical conductivity of the films. On the other hand, co-deposited C may hinder the grain growth of metal particles, resulting in the formation of nano-particles with a significantly large surface area. Since no chemical reaction between C and noble metals can proceed below 1700 K, noble metal particles can be stably present in a C matrix even at high temperatures.[15]

We have previously prepared Ir-C and Ru-C nano-composite films by MOCVD and investigated their microstructures and electrical/catalytic properties.[16,17] Since MOCVD is a thermally activated process, the grain growth of noble metal particles even in a C matrix inevitably occurred, particularly at a deposition temperature above 973 K.

In this study, Ru-C nano-composite films were prepared by plasma-enhanced CVD (PECVD) to obtain much smaller Ru particles dispersed uniformly in films and their microstructures and electrical properties were investigated.

2. Experimental

Figure 1 is a schematic diagram of a vertical cold-wall-type PECVD apparatus. A precursor of $Ru(dpm)_3$ (dipivaloylmethanate ruthenium, $Ru(C_{11}H_{19}O_2)_3$) was vaporized at 453 K and carried into a CVD chamber with Ar gas. Quartz ($10 \times 15 \times 0.5$ mm) plates and YSZ discs (10 mm in diameter) were used as substrates. Y_2O_3-ZrO_2 (8 mol%) powder (TOSOH, TZ-8YS) was sintered at 1573 K for 24 h to obtain YSZ discs. Deposition conditions were summarized in Table 1. The plasma power (P_M) and the deposition temperature (T_{dep}) are varied from 0.3 to 0.9 kW and 573 to 973 K, respectively. T_{dep} was measured by a thermocouple (K-type) attached to a substrate holder. The crystalline phase was investigated by X-ray diffraction (XRD). The composition was determined by energy dispersive X-ray spectroscopy

*Graduate Student, Tohoku University

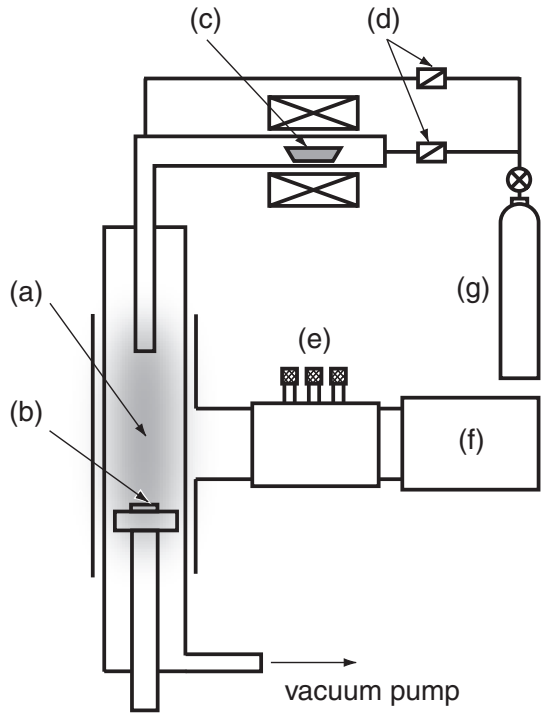

Fig. 1 Schematic diagram of a vertical cold-wall type PECVD apparatus: (a) plasma, (b) substrate, (c) precursor, (d) mass flow controller, (e) tuner, (f) microwave generator and (g) Ar gas.

Table 1 Deposition conditions.

Deposition temperature, T_{dep}/K	573–973
Microwave power, P_M/kW	0.1–0.9
Total gas pressure, P_{tot}/kPa	0.4
Precursor temperature, T_{Ru}/K	450
Ar carrier gas flow rate, $FR/10^{-7}$ m^3 s^{-1}	3.3
Deposition time, t/ks	0.6, 1.8

(EDS) and X-ray photoelectron spectroscopy (XPS). In the XPS analysis, the surface of specimens was sputtered with Ar ion at 2 kV for 15 min to eliminate the surface contamination of hydrocarbons. The microstructures were observed by a field-emitted scanning electron microscope (FE-SEM, JEOL JSM-6500FT) and a transmission electron microscope (TEM, JEOL JEM-3010). The electrical properties of Ru-C nano-composite films deposited as electrodes on YSZ substrates were investigated by AC impedance spectroscopy (Solatron 1260 and Solatron 1294) in the frequency range from 10^{-2} to 10^7 Hz and the temperature range from 473 to 873 K. The AC voltage was fixed at 0.1 V.

3. Results and Discussion

Figure 2 shows the XRD pattern of the Ru-C nano-composite film prepared at $P_M = 0.3$ kW and $T_{dep} = 573$ K. Broad peaks around $2\theta = 23^\circ$ and 43° were assigned to SiO_2 (substrate) and Ru (002). The average crystallite size of Ru calculated by the Scherrer equation[18] was 1.2 nm.

Figure 3 depicts the EDS spectrum of the Ru-C nano-composite film prepared at $P_M = 0.7$ kW and $T_{dep} = 973$ K. The peaks were assigned to C Kα, Ru Lα and Ru Lβ. The

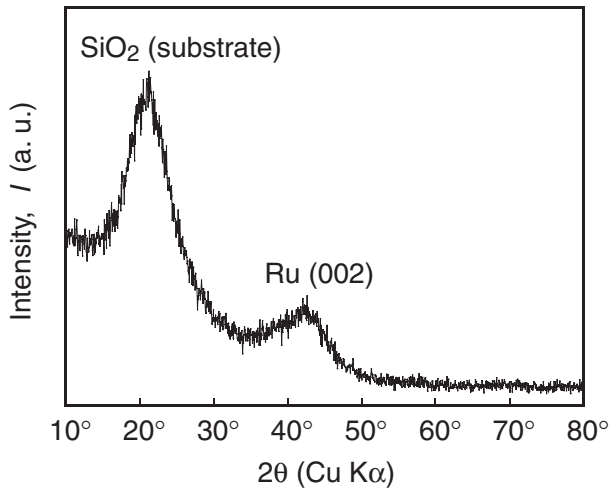

Fig. 2 XRD pattern of the Ru-C nano-composite film prepared at $P_M = 0.3$ kW and $T_{dep} = 573$ K.

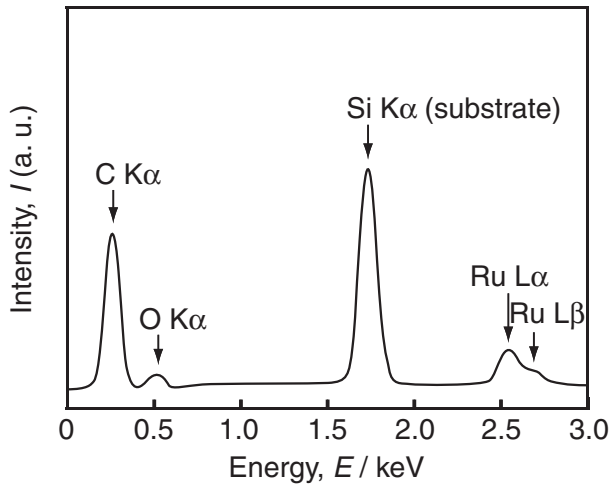

Fig. 3 EDS spectrum of the Ru-C nano-composite film prepared at $P_M = 0.7$ kW and $T_{dep} = 973$ K.

volume fraction of C was calculated as 0.90 from the intensity ratio between C Kα and Ru Lα and Ru Lβ. Figure 4 shows the effect of T_{dep} on the volume fraction of C at $P_M = 0.7$ kW. The volume fraction of C increased from 0.84 to 0.90 with increasing T_{dep} from 773 to 973 K.

Figure 5 presents the XPS spectrum of the Ru-C nano-composite film prepared at $P_M = 0.7$ kW and $T_{dep} = 973$ K. Although the binding energy of Ru $3d_{3/2}$ (284.1 eV) is close to that of C $1s_{1/2}$ (284.4 eV),[19–21] the peak around 284 eV can be deconvoluted into three components, namely, C 1s (contamination), C 1s (in the film) and Ru $3d_{3/2}$, where the intensity ratio of Ru $3d_{5/2}$ to Ru $3d_{3/2}$ peak was assumed to 1 : 1.45.[22] The volume fraction of C was estimated as being 0.88 to 0.93, which was almost in agreement with that by EDS.

Figure 6 depicts the surface and cross-sectional SEM images of Ru-C nano-composite films prepared at $T_{dep} =$ 973 K. The Ru-C nano-composite films prepared at $P_M = 0.7$ kW (Figs. 6(a), (b)) consisted of agglomerated grains of about 10 nm in diameter. The grain size increased with

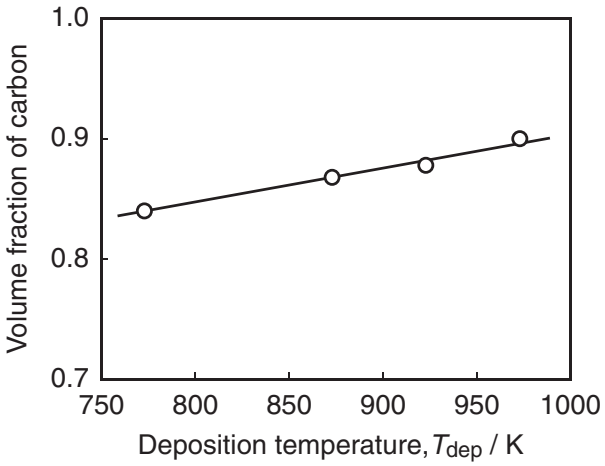

Fig. 4 Effect of T_{dep} on the volume fractions of C in the Ru-C nano-composite films.

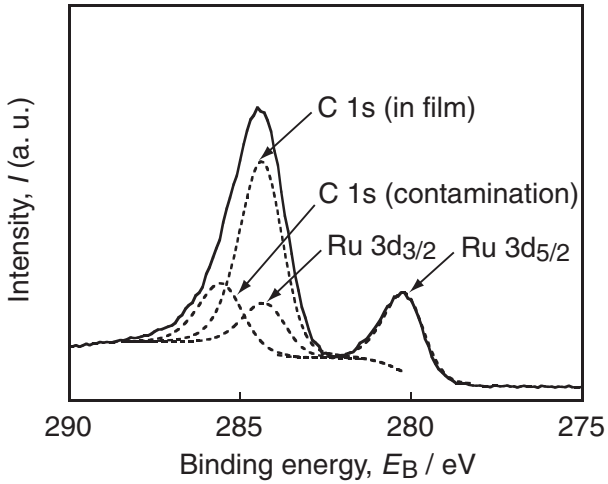

Fig. 5 XPS spectrum of Ru-C nano-composite film prepared at $P_M = 0.7$ kW and $T_{dep} = 973$ K. Broken lines are deconvoluted curves of Ru $3d_{5/2}$, Ru $3d_{3/2}$, C $1s_{1/2}$ (in film) and C $1s_{1/2}$ (contamination).

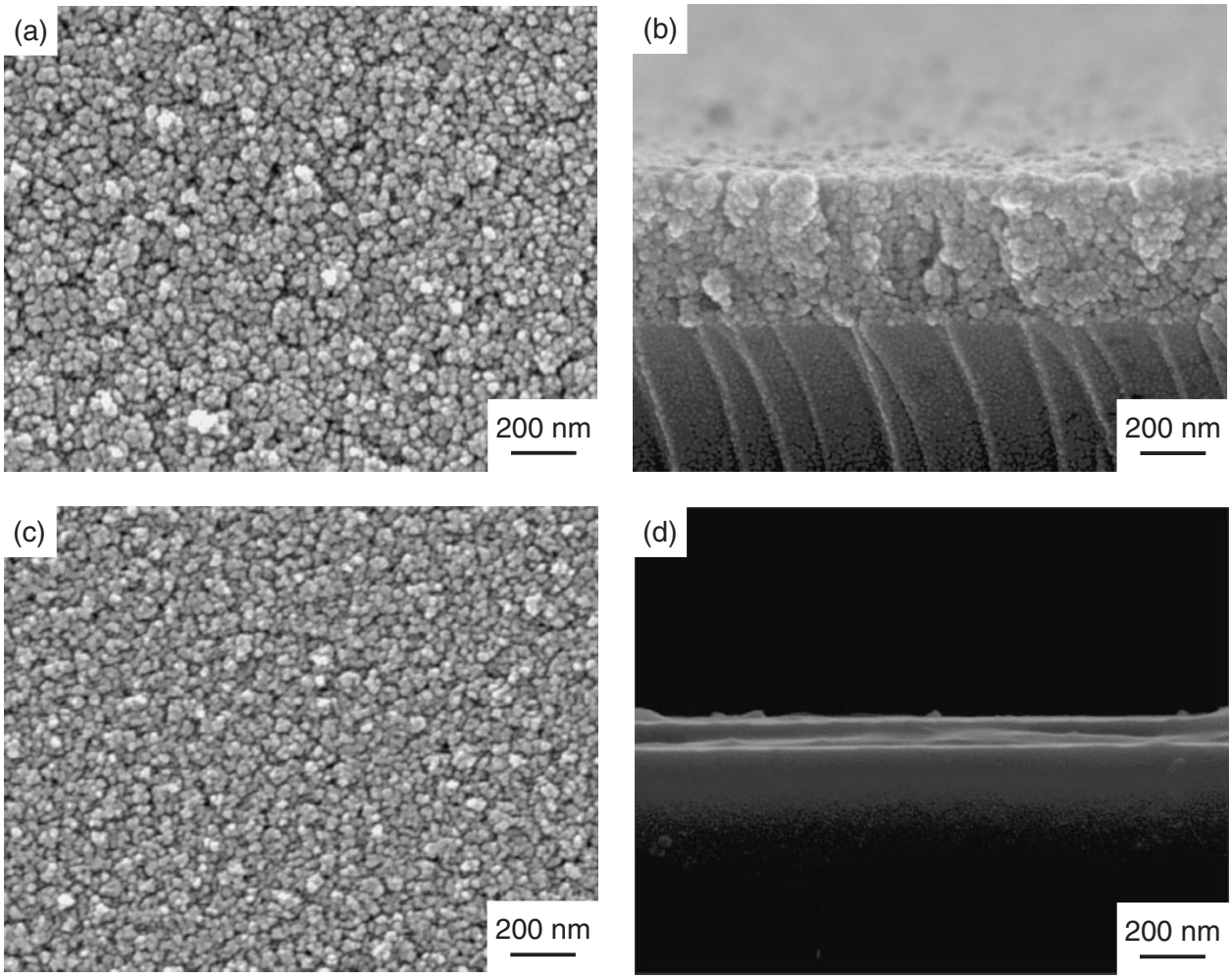

Fig. 6 Surface and cross-sectional SEM images of Ru-C nano-composite films prepared at (a) (b) $P_M = 0.7$ kW and $T_{dep} = 973$ K, (c) (d) $P_M = 0.3$ kW and $T_{dep} = 973$ K. (a) (c): surface, (b) (d): cross section.

increasing T_{dep} and was 20 nm at 973 K. The thickness of the films was about 500 nm. The thickness of the Ru-C nano-composite films prepared at $P_M = 0.3$ kW (Figs. 6(c), (d)) was 95 nm. Although the surface was similar to the agglomerated grain texture, the cross section was dense.

At $P_M < 0.3$ kW, metallic films were deposited on a chamber wall by which the microwave was reflected, resulting in destabilization of the plasma formation.

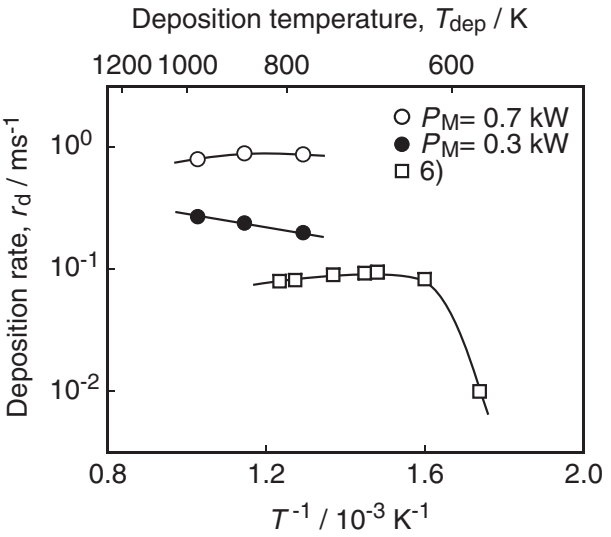

Fig. 7 Effect of T_{dep} on deposition rates of Ru-C nano-composite films by present PECVD and that of Ru films by MOCVD.[6)]

Figure 7 demonstrates the effect of T_{dep} on the deposition rates of Ru-C nano-composite films compared with those of Ru films prepared by conventional MOCVD[6)] using dicarbonylcyclopentadienylruthenium (II) dimer ($(C_5H_5Ru(CO)_2)_2$). The deposition rate by PECVD was about 10 times as high as that by MOCVD, almost independent of species T_{dep} over 600 K. The formation of volatile oxide (RuO_3, RuO_4) might have hindered the increase in deposition rate at higher T_{dep}.

Figure 8 depicts TEM images of the Ru-C nano-composite film prepared at $P_M = 0.5$ kW and $T_{dep} = 973$ K. Ru nano-particles of 2 to 3 nm in diameter were dispersed in an amorphous C matrix. The higher magnification of the Ru nano-particles (Fig. 8(b)) shows the atomic arrangement of rows of these particles with spacing of 0.27 nm, which was in agreement with the *d*-value of Ru (100) (0.2705 nm). The volume fraction of C estimated graphically from the TEM image was about 0.8, which was close to that calculated by EDS and XPS.

Figure 9 demonstrates the effect of deposition conditions (T_{dep} and P_M) on the Ru particle diameter estimated by TEM observations. The diameter increased from 2.5 to 3.5 nm with increasing T_{dep} (Fig. 9(a)), whereas the diameter had the maximum value of 3.5 nm at $P_M = 0.7$ kW (Fig. 9(b)). These diameters agreed with the Ru crystallite size estimated with the XRD pattern and were much smaller than those of Ru particles of 5–20 nm obtained by MOCVD.

The electrical properties of Ru-C nano-composite film prepared at $P_M = 0.7$ kW and $T_{dep} = 873$ K on YSZ substrates were evaluated as an electrode by AC impedance spectroscopy. The complex impedance of the YSZ electrolyte can be analyzed by three series components, namely, bulk (b), grain boundary (g) and interface (i), as depicted in Fig. 10. C and R denote associated capacitance and resistance, respectively. The interface component contains a non-linear diffusion process (Warburg process, W) in the electrode, and then W is included in the equivalent circuit. The usual infinite length diffusion process would be expressed as a linear line inclined 45° from the Z′ axis (not to a semicircle) as the interface component. On the other hand, in the case of a highly catalytic electrode, the 45° line would decline to a deformed semicircle.[23)]

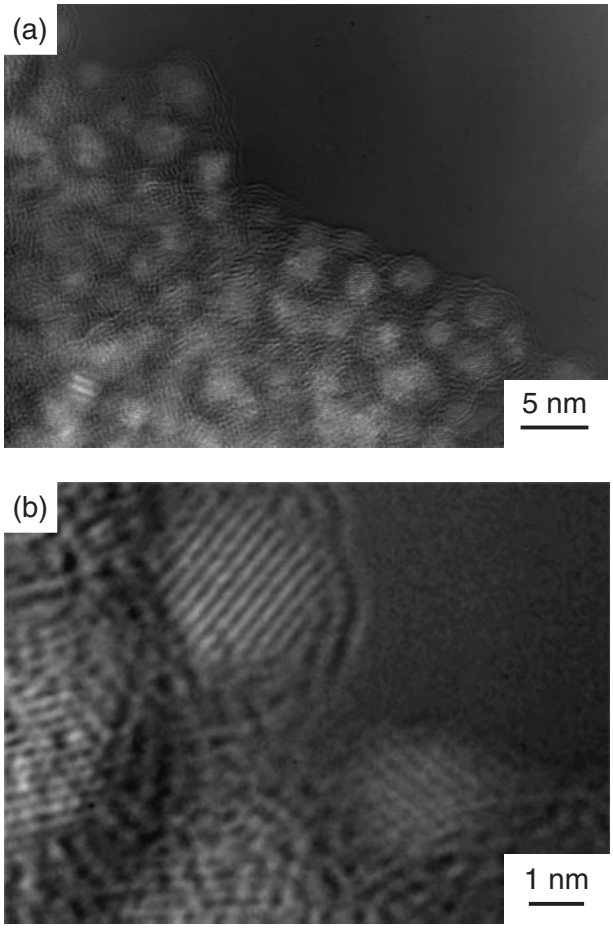

Fig. 8 TEM images of Ru-C nano-composite film prepared at $P_M = 0.5$ kW and $T_{dep} = 973$ K, (b) is a higher magnification of (a).

Figure 11 shows a complex impedance plot of the YSZ electrolyte using the Ru-C nano-composite film electrode prepared at $P_M = 0.7$ kW and $T_{dep} = 873$ K. The C_b, C_g and C_i values were 32 pF, 0.85 nF and 12 μF, respectively. Those values were well coincident with common bulk, grain boundary and interface contributions.[24–26)] The R_i is closely related to the charge transfer process at the interface, and the catalytic activity can often be evaluated from the reciprocal R_i ($1/\sigma_i$); the higher σ_i suggests the better catalytic activity of the electrode.

Figure 12 demonstrates the temperature dependence of σ_i ($= 1/R_i$) obtained from the third semicircle depicted in Fig. 11. The σ_i increased with increasing temperature, and was 0.2×10^{-3} Sm^{-1} at 500 K, significantly higher than that of conventional Pt paste electrode.[27)] The σ_i was almost the same among Ru-C nano-composite films with the different microstructure shown in Fig. 6. The activation energy of the σ_i was 70 kJ/mol. Yoon *et al.* studied the reaction at the YSZ/Pt interface[28)] and reported the relationship between the activation energy and the rate-controlling process. They reported the activation energy of 80 ± 5 kJ/mol at the high temperature region ($T > 1073$ K) and the low temperature

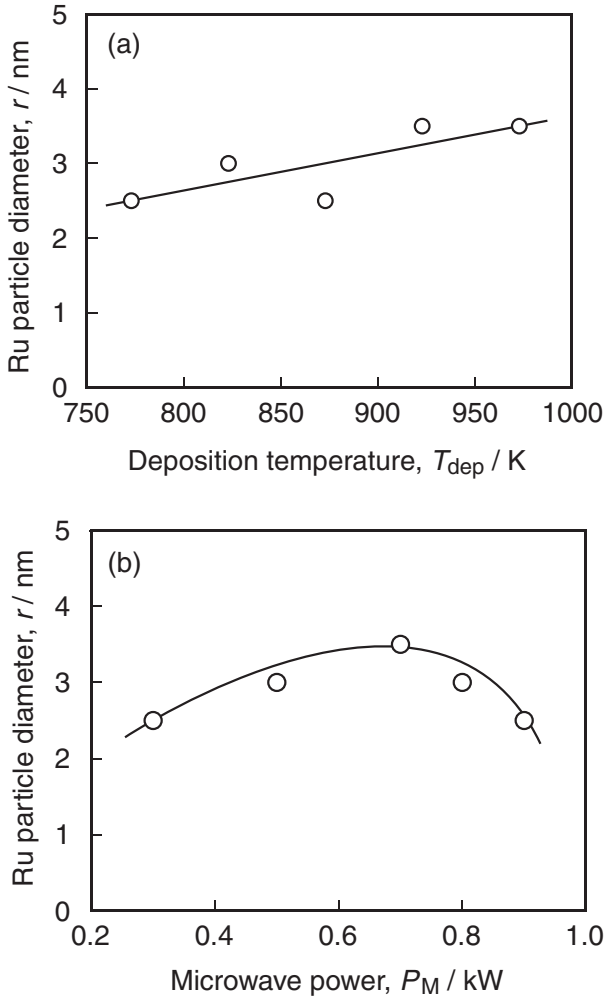

Fig. 9 Effects of deposition temperature (a) and microwave power on Ru particle diameter (b).

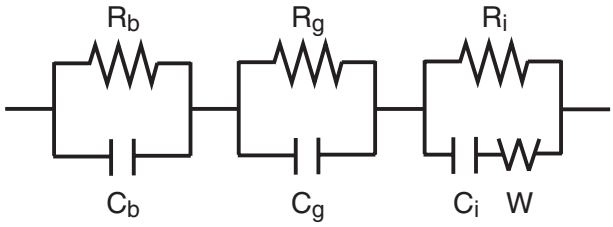

Fig. 10 An equivalent circuit for YSZ, C: capacitance, R: resistance, W: Warburg component.

region ($T < 973$ K) and concluded that the rate-controlling process was the migration process of oxygen vacancies to the triple phase boundary in the high temperature region and the dissociation reaction of oxygen molecules involving the charge transfer at triple phase boundary at the low temperature region. The activation energy of the Ru-C/YSZ cell was 70 kJ/mol in 493–873 K, which value was almost the same as the value of the Pt/YSZ cell, 1073–1273 K. The catalytic activity of the Ru-C nano-composite film obtained in the present study is possibly high enough to dissociate oxygen molecules, and then the migration of oxide vacancies to the triple phase boundary might be rate-controlling.

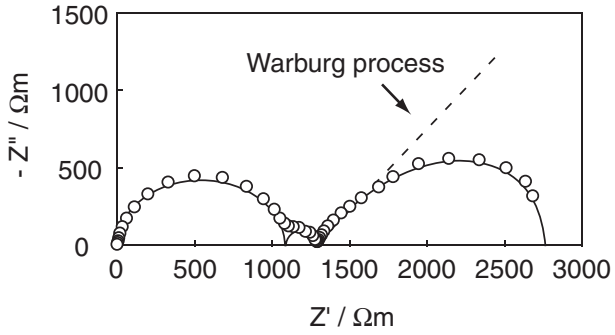

Fig. 11 Complex impedance plot of YSZ cell at 673 K using Ru-C nano-composite film electrodes prepared at $P_M = 0.7$ kW and $T_{dep} = 873$ K.

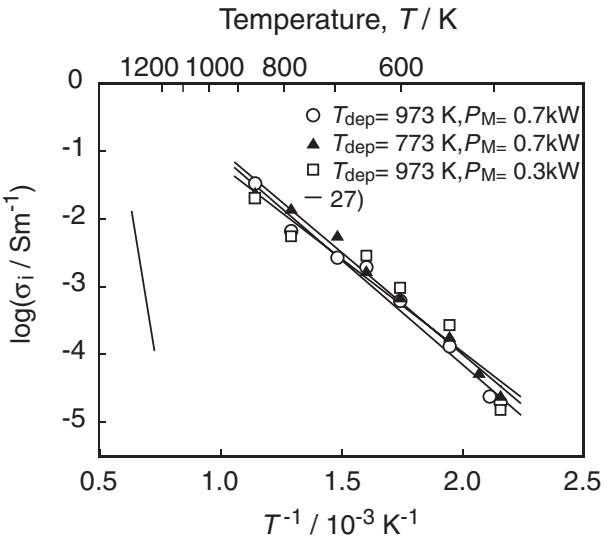

Fig. 12 Temperature dependence of interfacial electrical conductivity (σ_i) for YSZ using Ru-C nano-composite film electrodes.

4. Conclusions

Ru-C nano-composite films were prepared by PECVD. The films consisted of agglomerated grains of 10 to 20 nm in diameter, in which Ru nano-particles of 2.5 to 3.5 nm in diameter were dispersed in an amorphous C matrix. The volume fraction of C was 0.84 to 0.90. The interfacial conductivity (σ_i) of the YSZ solid electrolyte using the Ru-C nano-composite electrode was 0.2×10^{-3} Sm^{-1} at 500 K. The σ_i value was significantly higher than that of a conventional Pt paste electrode, suggesting excellent catalytic activity of the Ru-C nano-composite film. The activation energy of σ_i was about 70 kJ/mol, implying a process which limited the migration of oxygen vacancies to the triple phase boundary.

Acknowledgements

This work was conducted under the auspices of 21 century COE program and Asia CORE University program. The authors wish to thank N. Ohtsu (Advanced Research Center of Metallic Glasses, Institute for Materials Research, Tohoku University) for XPS analysis and E. Aoyagi and Y. Hayasaka

(Institute for Materials Research, Tohoku University) for FE-SEM and TEM observations. Furuya Metal, Japan and Lonmin, UK financially supported this work and provided $Ru(dpm)_3$ precursor.

REFERENCES

1) H. Obayashi and H. Okamoto: Solid State Ionics. **3–4** (1981) 631–634.
2) I. A. Toyashima and G. A. Somorjai: Catal. Rev. Sci. Eng. **19** (1979) 105–113.
3) C. M. Varma and A. J. Wilson: Phys. Rev. B **22** (1980) 3795–3804.
4) M. L. Green, M. E. Gross, L. E. Papa, K. J. Schoes and D. Brase: J. Electrochem. Soc. **132** (1985) 2677–2685.
5) K. C. Smith, Y. M. Sun, N. R. Mettlach, R. L. Hance and J. M. White: Thin Solid Films **376** (2000) 73–81.
6) Y. Senzaki, F. B. McCormick and W. L. Gladfelter: Chem. Mater. **4** (1992) 747–749.
7) W. Y. Cheng, L. S. Hong, J. C. Jiang, Y. Chi and C. C. Lin: Thin Solid Films **483** (2005) 31–37.
8) H. Schulz: Appl. Catal. A **186** (1999) 71–90.
9) O. Hinrichsen, F. Rosowski, M. Muhler and G. Ertl: Chem. Eng. Sci. **51** (1996) 1683–1690.
10) J. Aßmann, E. Löffler, A. Birkner and M. Muhler: Catal. Today **85** (2003) 235–249.
11) J. Ding, K. U. Chan, J. Ren and F. S. Xiao: Electrochim. Acta. **50** (2005) 3131–3141.
12) C. C. Chien and K. T. Jeng: Mater. Chem. Phys., in press.
13) K. T. Jeng, C. C. Chien, N. Y. Hsu, S. C. Yen, S. D. Chiou, S. H. Lin and W. M. Huang: J. Power Sources, in press.
14) C. Lim, R. G. Allen and K. Scott: J. Power Sources, in press.
15) Z. Kowalczyk, S. Jodzis and J. Sentek: Appl Catal. A: General **138** (1996) 83–91.
16) T. Goto, T. Ono and T. Hirai: Scripta Mater. **44** (2001) 1187–1190.
17) T. Kimura, G. Suzuki and T. Goto: J. Metastable Nanocrystal. Mater. **24–25** (2005) 589–592.
18) H. Borchert, E. V. Shevchenko, A. Robert, I. Mekis, A. Kornowski, G. Grübel and H. Weller: Langmuir **21** (2005) 1931–1936.
19) B. Folkesson: Acta Chem. Scand. **27** (1973) 287–302.
20) Y. Baer, P. F. Hedén, J. Hedman, M. Klasson, C. Nordling and K. Siegbahm: Phys. Scr. **1** (1970) 55–65.
21) D. N. Hendrickson, J. M. Hollander and W. L. Jolly: Inorg. Chem. **9** (1970) 612–615.
22) J. H. Scofield: J. of Electron Spectrosc. and Relat. Phenom. **8** (1976) 129–137.
23) J. E. Bauerle: J. Phys. Chem. Solids. **30** (1969) 2657–2670.
24) N. Matsui: Surf. Sci. **86** (1979) 353–358.
25) J. T. S. Irvine, D. C. Sinclair and A. R. West: Adv. Mater. **2** (1990) 132–138.
26) E. Schouler and M. Kleitz: J. Electroanal. Chem. **64** (1975) 135–142.
27) S. P. S. Badwal and H. J. de Bruin: Phys. Stat. Sol. (a) **54** (1979) 261–270.
28) S. P. Yoon, S. W. Nam, S. G. Kim, S. A. Hong and S. H. Hyun: J. Power Sources **115** (2003) 27–34.